Journal of Organometallic Chemistry 695 (2010) 1813–1823

Contents lists available at ScienceDirect

Journal of Organometallic Chemistry

journal homepage: www.elsevier.com/locate/jorganchem

Structural, spectral, and electrochemical investigations of *para*-tolyl-substituted oligogermanes

Monika L. Amadoruge [a], Erin K. Short [a], Curtis Moore [b], Arnold L. Rheingold [b], Charles S. Weinert [a,*]

[a] Department of Chemistry, Oklahoma State University, Stillwater, OK 74078, USA
[b] Department of Chemistry and Biochemistry, University of California, San Diego, La Jolla, CA 92093-0303, USA

ARTICLE INFO

Article history:
Received 2 February 2010
Received in revised form
14 April 2010
Accepted 16 April 2010
Available online 24 April 2010

Keywords:
Germanium
Oligogermanes
X-ray crystal structures
Cyclic voltammetry
Hydrogermolysis

ABSTRACT

The synthesis of four new oligogermanes containing *para*-tolyl-substituents has been achieved via the hydrogermolysis reaction, including the digermane $Tol_3GeGePh_3$, the trigermanes $Tol_3GeGePh_2GeTol_3$ and $Tol_3GeGeTol_2GeTol_3$, and the tetragermane $Tol_3GeGePh_2GePh_2GeTol_3$ (Tol = *p*-$CH_3C_6H_4$). These four oligogermanes have been structurally characterized and their structures have been compared with those of their *per*-phenyl-substituted analogs. The digermane $Tol_3GeGePh_3$ exhibits an unusually short Ge–Ge bond distance of 2.408(1) Å. The four *para*-tolyl-substituted oligogermanes have also been characterized by UV/visible spectroscopy and cyclic voltammetry. The expected red shift in the absorbance maximum with increasing catenation was observed for this series of compounds. Their cyclic voltammograms each contain $n - 1$ irreversible oxidation waves (n = the number of Ge atoms), which is atypical since oligogermanes generally exhibit only one irreversible oxidation wave regardless of the degree of catenation.

1. Introduction

The synthesis of catenated compounds of the heavier group 14 elements containing element–element single bonds is of significant interest since these materials represent the heavy analogs of hydrocarbons. However, in contrast to their carbon-containing congeners, catenated compounds of silicon, germanium, and tin exhibit σ-delocalization, where the constituent electrons of the element–element single bonds are delocalized across the entire element–element backbone [1–8]. This can result in interesting optical and electronic properties, including thermochromism, conductivity, and non-linear optical attributes. However, while silicon- [9–19] and tin-containing [4,5,20–35] catenates have received considerable attention, an understanding of their germanium-containing analogs is not as well developed. This is due, in part, to the lack of suitable synthetic methods for the preparation of catenated germanium compounds, which has until recently precluded a detailed investigation into the structure/property relationships in these systems [36–40].

Rather than focusing on polymeric systems that have a distribution of molecular weights and therefore contain mixtures of products, we have endeavored to develop a synthetic methodology that will allow the synthesis of discrete oligogermanes having a well-defined composition. We have used the hydrogermolysis reaction, either alone or in conjunction with a germanium hydride protection/deprotection strategy, to prepare a library of oligogermanium compounds having between two and seven germanium atoms in the Ge–Ge backbone [41–45]. Our synthetic methodology can be employed for the systematic variation of not only the number of germanium atoms in the Ge–Ge backbone but also of the organic substituents attached to the germanium atoms in the chain. This was not possible using other previously reported synthetic methods, and we have prepared both linear [41,42,44,45] and branched [43] oligogermane systems using this method. It has been demonstrated that both the number of catenated germanium atoms and the electronic attributes of the attached organic substituents affect the relative energies of the frontier orbitals in these systems. This has been achieved by characterizing the oligogermane systems using UV/visible spectroscopy and cyclic voltammetry, in conjunction with computational (DFT) studies.[42] We have shown that the magnitude of the $\sigma \rightarrow \sigma^*$ electronic transition, which corresponds to the promotion of an electron from the HOMO σ-bonding orbital to the LUMO σ*-antibonding orbital, decreases upon increasing the Ge–Ge chain length and/or by increasing the number of inductively electron-donating organic substituents. In general, this effect results from the destabilization of the HOMO, and these two structural modifications also diminish the oxidation potential of these systems. The oxidation waves

* Corresponding author. Tel.: +1 405 744 6543.
E-mail address: weinert@chem.okstate.edu (C.S. Weinert).

0022-328X/$ – see front matter © 2010 Elsevier B.V. All rights reserved.
doi:10.1016/j.jorganchem.2010.04.015

exhibited in the cyclic voltammograms of all oligogermanes observed to date are irreversible, indicating that a chemical reaction is occurring after the oxidation event [42,46,47].

The majority of the oligogermanes we have prepared in our laboratory, with the exception of several phenyl-substituted digermanes and the branched tetragermane $(Ph_3Ge)_3GePh$, are either liquids or amorphous solids at room temperature. The majority of oligogermanes Ge_nR_{2n+2} that have been characterized using X-ray crystallography ($n = 2$–5) contain phenyl substituents, although the yields of these products are generally low (0.5–45%) [20,39,41,44,45,48–51]. Due to our desire to use our oligogermane systems as precursors for the synthesis of germanium-based nanomaterials, we were interested in preparing new systems that could be structurally characterized. The present work focuses on the preparation of *para*-tolyl-substituted oligogermanes, where the *para*-methyl group of the tolyl substituents can be used for an initial assessment of the purity of the products using ^{1}H NMR spectroscopy. We have prepared and structurally characterized four new tolyl-substituted oligogermanes containing between two and four germanium atoms in the chain, and these compounds have been further characterized using NMR, infrared, and UV/visible spectroscopy, cyclic voltammetry, and elemental analysis. We have observed, for the first time, multiple irreversible oxidation events in the cyclic voltammograms of these oligogermanes, and have postulated the pathway of decomposition after the oxidation event takes place.

2. Results and discussion

2.1. Syntheses and X-ray crystal structures

The germanium starting materials Tol_3GeCl and Tol_2GeBr_2 (Tol = *p*-$H_3CC_6H_4$) were prepared by the action of TolMgCl on $GeCl_4$ or TolMgBr on $GeBr_4$ (respectively) under carefully controlled reaction conditions to prevent the formation of oligogermanes. While the reaction of $GeCl_4$ with 3 equiv. of TolMgCl yielded primarily the desired triaryl product Tol_3GeCl, the preparation of the diaryl material Tol_2GeBr_2 was complicated by the concomitant formation of Tol_3GeBr and $TolGeBr_3$. Separation of the three components of the product mixture proved difficult, and as a result the product mixture was treated directly with excess $LiAlH_4$ to yield a mixture of the corresponding arylgermanium hydrides R_nGeH_{4-n} ($n = 1$–3). The three hydrides could be readily separated by fractional vacuum distillation and Tol_2GeH_2 was obtained in 8% yield based on $GeBr_4$. The ^{1}H NMR spectrum of Tol_2GeH_2 contains a singlet at δ 5.22 ppm corresponding to the two equivalent hydridic protons, and the IR spectrum of this material contains a symmetric Ge–H stretching band at 2050 cm^{-1}. The amide reagent Tol_3GeNMe_2 was prepared from the salt metathesis reaction of Tol_3GeCl with $LiNMe_2$ in 76% yield, and the ^{1}H NMR spectrum of this material exhibits a singlet at δ 2.84 ppm corresponding to the protons of the amide methyl groups.

The digermane $Tol_3GeGePh_3$ (**1**) and the trigermanes $Tol_3GeGePh_2GeTol_3$ (**2**) and $Tol_3GeGeTol_2GeTol_3$ (**3**) were prepared using the amide Tol_3GeNMe_2 via the hydrogermolysis reaction in CH_3CN solvent (Scheme 1). As previously described [41–45], the germanium amide reagent Tol_3GeNMe_2 reacts *in situ* with the CH_3CN solvent to generate the α-germyl nitrile Tol_3GeCH_2CN, which contains a labile Ge–C bond and is the active species in the germanium–germanium bond forming process. The ^{1}H NMR spectra of **1** and **2** exhibit similar patterns in the aromatic region that are consistent with expected chemical shift values. In both compounds resonances for the *ortho*-protons of the tolyl rings are shifted downfield relative to those for the *ortho*-protons of the phenyl rings, while resonances for the *meta*-protons appear upfield relative to those of the phenyl groups. In addition, resonances for the *ipso*-carbons of the tolyl groups in the ^{13}C NMR spectra of **1** and **2** appear downfield relative to those of the phenyl groups. Singlets for the methyl protons of **1** and **2** were observed at δ 2.02 and 2.07 ppm, respectively, while the *per*-tolyl-substituted trigermane **3** exhibits two methyl group resonances at δ 2.09 and 1.99 ppm, where the singlet corresponding to the central tolyl substituents appears upfield at δ 1.99 ppm.

The crystal structures of **1**–**3** were determined and an ORTEP diagram of **1**·2C_6H_6 is shown in Fig. 1 while selected bond distances and angles are collected in Table 1. Curiously, the Ge–Ge bond distance in **1** measures 2.408(1) Å, which is shorter than the reported Ge–Ge bond length in the related perphenyl digermane $Ph_3GeGePh_3\cdot 2C_6H_6$ (**4**·2C_6H_6) of 2.446(1) Å [48], as well as that in the unsolvated form of **4** (2.437(2) Å) [52]. A survey of twenty-five structurally characterized digermanes [41,44,45,48,49,51–67] reveals that the Ge–Ge bond distance in **1** is the third shortest Ge–Ge bond length to be reported, where only $Cl_3CCOOPh_2GeGePh_2OOCCCl_3$ (**5**) [51] and (2,6-$Dipp_2C_6H_3$)H_2GeGeH_2($C_6H_3Dipp_2$-2,6) (Dipp = 2,6-di*iso*propylphenyl) [58] have shorter bond lengths of 2.393(2) and 2.402(1) Å, respectively. The short bond length in the latter compound is not surprising despite the presence of the bulky aryl groups at each germanium atom, since the other two

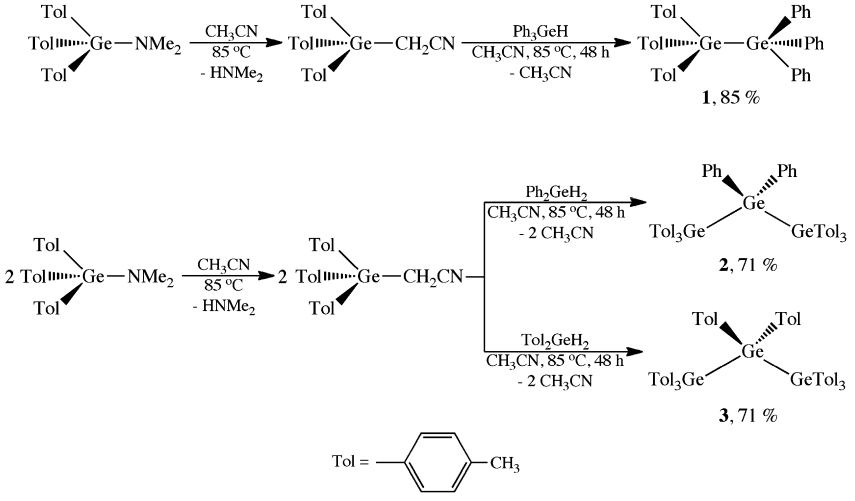

Scheme 1. Syntheses of $Tol_3GeGePh_3$ (**1**), $Tol_3GeGePh_2GeTol_3$ (**2**), and $Tol_3GeGeTol_2GeTol_3$ (**3**).

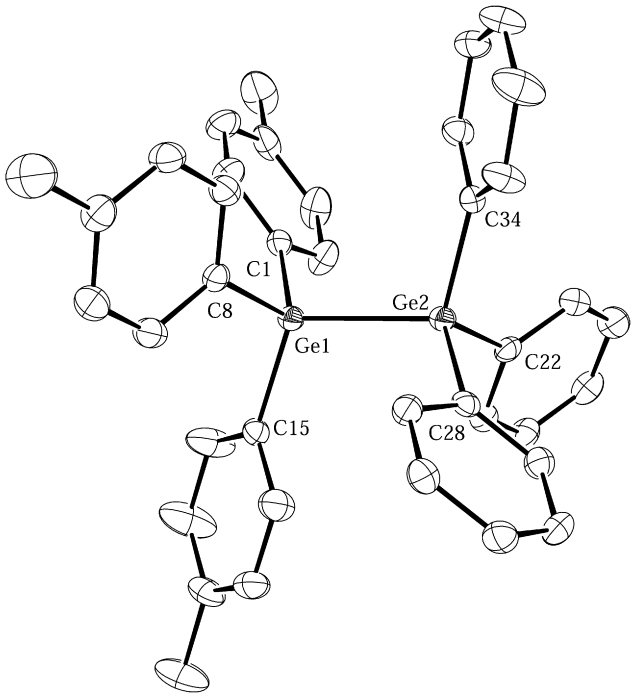

Fig. 1. ORTEP diagram of $Tol_3GeGePh_3 \cdot 2C_6H_6$ (**1**$\cdot 2C_6H_6$). Thermal ellipsoids are drawn at 50% probability.

substituents are sterically unencumbering hydrogen atoms. The bond length in **5** is constricted because the carbonyl oxygen atoms in each of the trichloroacetato ligands are coordinated to the opposite germanium atom to yield a hypervalent five-coordinate Ge center in each case [51]. The structure of $Ge_2Tol_6 \cdot C_6H_6$ was recently determined and this compound also has a short Ge–Ge distance that measures 2.419(1) Å [68].

The short Ge–Ge bond distances in **1**$\cdot 2C_6H_6$ and $Ge_2Tol_6 \cdot C_6H_6$ can be attributed to electronic effects, since the *para*-methyl group of the tolyl substituents presumably renders the germanium atoms more electron rich via inductive effects relative to a triphenyl-substituted germanium center. However, the constriction of the Ge–Ge bond distance in **1**$\cdot 2C_6H_6$ and $Ge_2Tol_6 \cdot C_6H_6$ is drastic compared to that in $Ph_3GeGePh_3 \cdot 2C_6H_6$, and similar short Ge–Ge bond lengths were not observed in **2**$\cdot C_7H_8$ or **3**$\cdot C_7H_8$ (*vide infra*). However, steric effects in the trigermanes **2**$\cdot C_7H_8$ and **3**$\cdot C_7H_8$ are greater than those in **1**$\cdot 2C_6H_6$ and $Ge_2Tol_6 \cdot C_6H_6$, and this presumably counteracts the electronic effects of the *para*-tolyl groups. Crystal packing effects also could contribute to the contracted Ge–Ge distances in **1**$\cdot 2C_6H_6$ and $Ge_2Tol_6 \cdot C_6H_6$, but it is unlikely that this solely results in the drastic shortening of the Ge–Ge distances in these two digermanes.

The structure of the trigermane **2**$\cdot C_7H_8$ is shown in Fig. 2 and selected bond distances and angles are collected in Table 2.

Table 1
Selected bond distances (Å) and angles (deg) for $Tol_3GeGePh_3 \cdot 2C_6H_6$ (**1**$\cdot 2C_6H_6$).

Ge(1)–Ge(2)	2.408(1)	C(8)–Ge(1)–C(15)	108.94(9)
Ge(1)–C(1)	1.942(2)	C(22)–Ge(2)–C(28)	109.89(9)
Ge(1)–C(8)	1.942(2)	C(22)–Ge(2)–C(34)	110.32(9)
Ge(1)–C(15)	1.935(2)	C(28)–Ge(2)–C(34)	109.97(8)
Ge(2)–C(22)	1.941(2)	C(1)–Ge(1)–Ge(2)	108.47(7)
Ge(2)–C(28)	1.940(2)	C(8)–Ge(1)–Ge(2)	109.72(7)
Ge(2)–C(34)	1.939(2)	C(15)–Ge(1)–Ge(2)	110.30(7)
		C(22)–Ge(2)–Ge(1)	109.18(7)
C(1)–Ge(1)–C(8)	109.64(9)	C(28)–Ge(2)–Ge(1)	110.47(7)
C(1)–Ge(1)–C(15)	109.76(9)	C(34)–Ge(2)–Ge(1)	106.97(7)

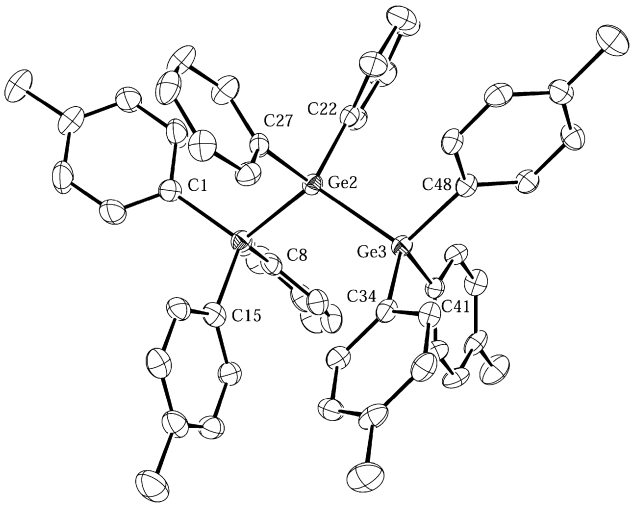

Fig. 2. ORTEP diagram of $Tol_3GeGePh_2GeTol_3 \cdot C_7H_8$ (**2**$\cdot C_7H_8$). Thermal ellipsoids are drawn at 50% probability.

Structurally characterized linear trigermanes are rare, and to our knowledge the structures of only six other such species have been previously reported [6,39,69–72]. The average Ge–Ge bond distance in **2**$\cdot C_7H_8$ is 2.4328(5) Å, which is shorter than the average Ge–Ge bond length in Ge_3Ph_8 (**6**, 2.440(2) Å) [39] but is similar to the average Ge–Ge bond distance of 2.429(1) in $Ph_3GeGeMe_2GePh_3$ (**7**) [69]. However, the contraction of the Ge–Ge bond lengths in **2**$\cdot C_7H_8$ compared to those in **6** is not as pronounced as that observed between **1**$\cdot 2C_6H_6$ and $Ph_3GeGePh_3$, further suggesting that interplay of electronic and steric effects in the trigermane **2**$\cdot C_7H_8$ have a combined effect on the Ge–Ge bond distance. The Ge–Ge–Ge bond angle at Ge(2) in **2**$\cdot C_7H_8$ measures 114.80(2)°, which is more acute that those in both **6** (121.3(1)°) [39] and **7** (120.3(1)°) [69] but is similar to those in the halide-substituted trigermanes $XBu^t_2GeGeBu^t_2GeBu^t_2X$ (X = Br [72], 113.6(1)°; X = I [71], 115.4(1)°). The C(22)–Ge(2)–C(28) bond angle in **2**$\cdot C_7H_8$ which measures 106.2(1)° is also more acute than the corresponding bond angle at the central germanium atom in both **6** (108.7(4)°) [39] and **7** (109.2(2)°) [69], which can be attributed to the steric effects of the six terminal tolyl groups.

The structure of the *per*-tolyl-substituted trigermane **3**$\cdot C_7H_8$ is shown in Fig. 3 and selected bond distances and angles are given in Table 3. The Ge–Ge bond distances in **3**$\cdot C_7H_8$ are longer than those in **2**$\cdot C_7H_8$ and **7** due to the additional steric crowding imposed by the two central tolyl substituents, and the average Ge–Ge bond

Table 2
Selected bond distances (Å) and angles (deg) for $Tol_3GeGePh_2GeTol_3 \cdot C_7H_8$ (**2**$\cdot C_7H_8$).

Ge(1)–Ge(2)	2.4318(5)	C(22)–Ge(2)–C(28)	106.2(1)
Ge(2)–Ge(3)	2.4338(4)	C(34)–Ge(3)–C(41)	108.7(1)
Ge(1)–C(1)	1.958(3)	C(34)–Ge(3)–C(48)	107.6(1)
Ge(1)–C(8)	1.959(3)	C(41)–Ge(3)–C(48)	109.0(1)
Ge(1)–C(15)	1.966(3)	C(1)–Ge(1)–Ge(2)	106.7(8)
Ge(2)–C(22)	1.958(3)	C(8)–Ge(1)–Ge(2)	117.36(9)
Ge(2)–C(28)	1.955(3)	C(15)–Ge(1)–Ge(2)	108.52(9)
Ge(3)–C(34)	1.957(3)	C(22)–Ge(2)–Ge(1)	111.50(9)
Ge(3)–C(41)	1.945(3)	C(28)–Ge(2)–Ge(1)	113.93(8)
Ge(3)–C(48)	1.944(3)	C(22)–Ge(2)–Ge(3)	105.28(8)
		C(28)–Ge(2)–Ge(3)	113.93(8)
Ge(1)–Ge(2)–Ge(3)	114.80(2)	C(34)–Ge(3)–Ge(2)	117.53(8)
C(1)–Ge(1)–C(8)	110.0(1)	C(41)–Ge(3)–Ge(2)	106.95(8)
C(1)–Ge(1)–C(15)	108.1(1)	C(48)–Ge(3)–Ge(2)	106.81(8)
C(8)–Ge(1)–C(15)	105.8(1)		

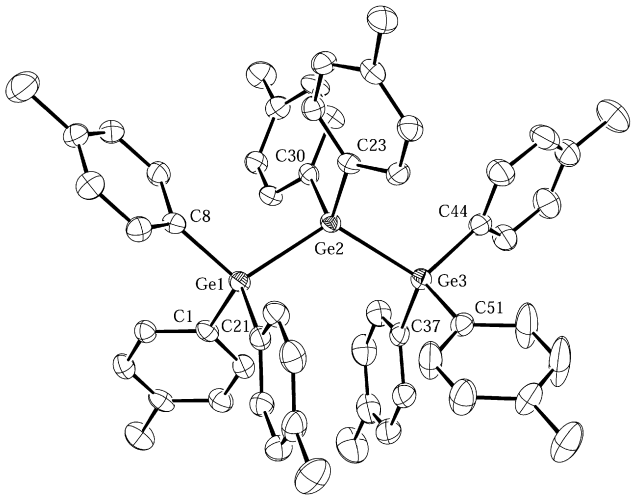

Fig. 3. ORTEP diagram of $Tol_3GeGeTol_2GeTol_3 \cdot C_7H_8$ ($3 \cdot C_7H_8$). Thermal ellipsoids are drawn at 50% probability.

distance in $3 \cdot C_7H_8$ is 2.4404(5) Å. However, this value is nearly identical to that of trigermane **6** (2.440(2) Å) [39]. The central Ge–Ge–Ge bond angle in $3 \cdot C_7H_8$ of 117.54(1)° is more acute than those in both **6** (121.3(1)°) [39] and **7** (120.3(1)°) [69], but is more obtuse than the corresponding angle in $2 \cdot C_7H_8$ (114.80(2)°). The central C(23)–Ge(2)–C(30) angle in $3 \cdot C_7H_8$ measures 106.45(9)°, which is slightly more obtuse than that in $2 \cdot C_7H_8$ (106.2(1)°), but is more acute than the corresponding angles in both **6** (108.7(4)°) [39] and **7** (109.2(2)°) [69]. Therefore, the effects resulting from the presence of tolyl groups versus phenyl groups at the central germanium atom in the three trigermanes $2 \cdot C_7H_8$, $3 \cdot C_7H_8$, and **6** depend on the identity of the substituents attached to the terminal germanium atoms. The trigermane $3 \cdot C_7H_8$, which contains eight tolyl substituents and thus is the most sterically encumbered of these three molecules, has the longest Ge–Ge bond distances but intermediate Ge–Ge–Ge and C–Ge–C bond angles at the central germanium atom. The trigermane **7**, which contains sterically unencumbering methyl substituents at the central germanium atom, has the shortest Ge–Ge bond distances among the three molecules and the most obtuse bond angles at the central germanium atom.

The synthesis of the tetragermane $Tol_3GeGePh_2GePh_2GeTol_3$ (**11**) was achieved in four steps starting from hexaphenyldigermane (Scheme 2). Using a variation of a published procedure, a single phenyl group was cleaved from each germanium atom in $Ph_3GeGePh_3$ (**4**) using trichloroacetic acid to yield the 1,2-trichloroacetato derivative **5** [51], and this was subsequently converted to the 1,2-dichloride **8** using hydrochloric acid [51]. The synthesis of **8** by the action of anhydrous HCl on $Ph_3GeGePh_3$ under pressure has also been described, which also lead to the formation of $Cl_2PhGeGePhCl_2$ (**9**). [55]. Treatment of **8** with $LiAlH_4$ furnished the 1,2-dihydride **10** in 79% yield. The ^1H NMR spectrum of **10** contains a singlet for the two equivalent hydridic protons at δ 5.58 ppm, and the Ge–H stretching frequency was observed at 2033 cm^{-1} in the IR spectrum of **10**. The synthesis of **10** has been achieved by other methods [73–75], including by the hydrolysis of Ph_2GeHLi [75] and also by the catalytic dehydrocoupling of Ph_2GeH_2 [74], and the spectral data obtained for **10** agree with the reported values. The tetragermane **11** was prepared from **10** and two equivalents of Tol_3GeNMe_2 in 80% yield via the hydrogermolysis reaction in CH_3CN, which again proceeds via the *in situ* generation of the reactive Tol_3GeCH_2CN intermediate. Similar to what was observed in the ^1H NMR spectra of **1** and **2**, resonances for the *ortho*-protons of the tolyl substituents of **11** are shifted downfield from those of the phenyl substituents while those of for the *meta*-protons are shifted upfield.

Structurally characterized linear tetragermanes are rare [39,69–72,76], and compounds that have been characterized by this method include $Ge_4Ph_{10} \cdot 2C_6H_6$ ($12 \cdot 2C_6H_6$) [39], 1,4-dichloro-octaphenyltetragermane [70], and 1,4-diiodo-octaphenyltetragermane [76]. An ORTEP diagram of the tetragermane **11** is shown in Fig. 4 and selected bond distances and angles for **11** are collected in Table 4. Compound **11** crystallizes with two independent molecules in the unit cell, where one of the molecules (molecule 1) is completely ordered and the other (molecule 2) is disordered. Both molecules of **11** are located on a crystallographic inversion center, and the germanium atoms of molecule 2 are disordered over two positions with occupancies of 85.6 and 14.4%. The bond distances given for molecule 2 are a weighted average of the two positions. The average Ge–Ge bond distance in **11** is 2.455 (3) Å which is somewhat shorter to the average Ge–Ge bond length in the perphenyl-substituted tetragermane $12 \cdot 2C_6H_6$ (2.462 (2) Å) [39].

As observed for the digermane $1 \cdot 2C_6H_6$ and the trigermanes $2 \cdot C_7H_8$ and $3 \cdot C_7H_8$ versus their perphenyl analogs, the steric and electronic effects of the tolyl groups in **11** versus the phenyl groups in $12 \cdot 2C_6H_6$ have an effect on the structural parameters. The terminal Ge–Ge bonds in both molecules of **11** (2.4490(8) and 2.460(3) Å) are shorter than those in the perphenyl tetragermane $12 \cdot 2C_6H_6$ (2.463(2) Å) [39], and the internal Ge–Ge distances in the molecules of **11** (2.457(1) and 2.448(3) Å) are also shorter than that of $12 \cdot 2C_6H_6$ (2.461(3) Å) [39]. Furthermore, the Ge–Ge–Ge bond angle in both molecules of **11** (115.53 (3) and 118.9(2)°) are more acute than that in $12 \cdot 2C_6H_6$ (121.3 (1)°) [39].

The overall geometry of **11** approximates that of *n*-butane, and is also similar to that of the tetragermane $12 \cdot 2C_6H_6$. Torsion angles for molecule 1 of **11** about the Ge(1)–Ge(2) and Ge(2)–Ge(2^i) bonds are collected in Table 5. The two terminal Tol_3Ge- groups in molecule 1 are disposed in an *anti*-conformation about the central Ge (2)–Ge(2^i) bond and the dihedral angle is exactly 180°, and the environment about the central Ge(2)–Ge(2′) bond in molecule 1 of **11** is symmetric due to the presence of a crystallographic inversion center. However, although the phenyl group containing C(8) and Ge (2′) are arranged in an approximate *anti*-conformation about the Ge (1)–Ge(2) bond, the dihedral angle between C(8) and Ge(2′) deviates from the ideal value of 180° by 13.2°. The structure of $12 \cdot 2C_6H_6$ exhibits a similar arrangement along the terminal Ge(1)–Ge(2) bond, but the dihedral angle in $12 \cdot 2C_6H_6$ is distorted by only 7.4°, and the greater distortion in **11** is attributed to the increased steric bulk of the tolyl substituents.

Table 3
Selected bond distances (Å) and angles (deg) for $Tol_3GeGeTol_2GeTol_3 \cdot C_7H_8$ ($3 \cdot C_7H_8$).

Ge(1)–Ge(2)	2.4450(4)	C(23)–Ge(2)–C(30)	106.45(9)
Ge(2)–Ge(3)	2.4359(5)	C(37)–Ge(3)–C(44)	107.0(1)
Ge(1)–C(1)	1.951(2)	C(37)–Ge(3)–C(51)	108.8(1)
Ge(1)–C(8)	1.951(2)	C(44)–Ge(3)–C(51)	107.4(1)
Ge(1)–C(21)	1.953(2)	C(1)–Ge(1)–Ge(2)	114.30(7)
Ge(2)–C(23)	1.958(2)	C(8)–Ge(1)–Ge(2)	108.32(6)
Ge(2)–C(30)	1.960(2)	C(21)–Ge(1)–Ge(2)	109.24(6)
Ge(3)–C(37)	1.950(2)	C(23)–Ge(2)–Ge(1)	106.21(6)
Ge(3)–C(44)	1.962(2)	C(30)–Ge(2)–Ge(1)	108.76(6)
Ge(3)–C(51)	1.949(2)	C(23)–Ge(2)–Ge(3)	109.94(7)
		C(30)–Ge(2)–Ge(3)	107.42(7)
Ge(1)–Ge(2)–Ge(3)	117.54(1)	C(37)–Ge(3)–Ge(2)	109.16(7)
C(1)–Ge(1)–C(8)	108.33(9)	C(44)–Ge(3)–Ge(2)	110.08(7)
C(1)–Ge(1)–C(21)	108.02(9)	C(51)–Ge(3)–Ge(2)	114.09(7)
C(8)–Ge(1)–C(21)	108.5(1)		

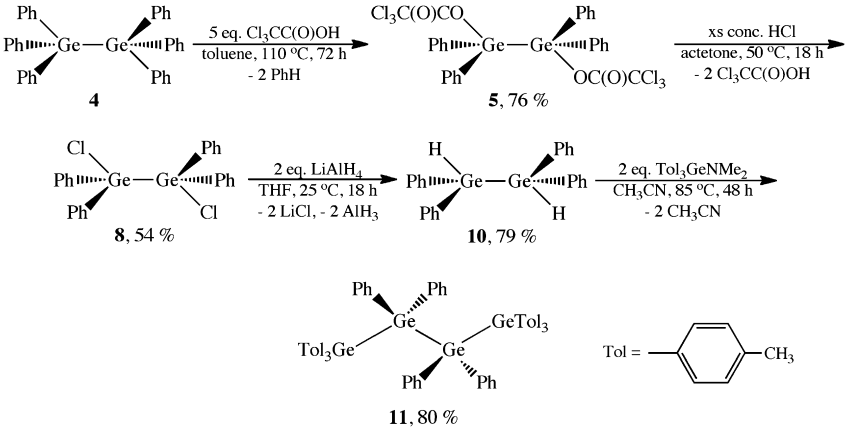

Scheme 2. Synthesis of $Tol_3GeGePh_2GePh_2GeTol_3$ (**11**).

2.2. UV/visible spectra and cyclic voltammetry

The series of four oligogermanes **1**–**3** and **11** were characterized using cyclic voltammetry in CH_2Cl_2 solution with 0.1 M $[Bu_4N][PF_6]$ as the supporting electrolyte. Voltammograms for each of the four species are shown in Fig. 5, average values for the oxidation waves for four separate runs and Ge–Ge bond distance data are collected in Table 6, and the proposed electrochemical decomposition pathways for **1**–**3** and **11** are shown in Scheme 3. The voltammograms for each of these Ge_nAr_{2n+2} compounds exhibit a total of $n - 1$ irreversible oxidation waves. This is significant, since oligogermanes that have been previously characterized by this method typically exhibit only one irreversible oxidation wave [42,46,47,77] due to decomposition of the oligogermane after the oxidation event occurs. However, the multiple waves observed for **2**, **3**, and **11** suggest that in the case of these three compounds, the product generated after oxidation is stable and undergoes either one (compounds **2** and **3**) or two (compound **4**) subsequent one-electron oxidation processes.

The oxidation potentials among the three digermanes **1**, Ge_2Tol_6, and Ge_2Ph_6 can be correlated with the Ge–Ge bond distances in these compounds. The single irreversible oxidation wave for **1** was observed at 1483 ± 17 mV, and this can be compared to that of a commercial sample of Ge_2Ph_6 (1958 ± 19 mV) and a sample of Ge_2Tol_6 (1757 ± 18 mV) prepared from Tol_3GeH and Tol_3GeNMe_2. Compound **1** exhibits the least positive oxidation potential among these three species and also has the shortest Ge–Ge bond distance. The electronic and steric attributes of the substituents both have an

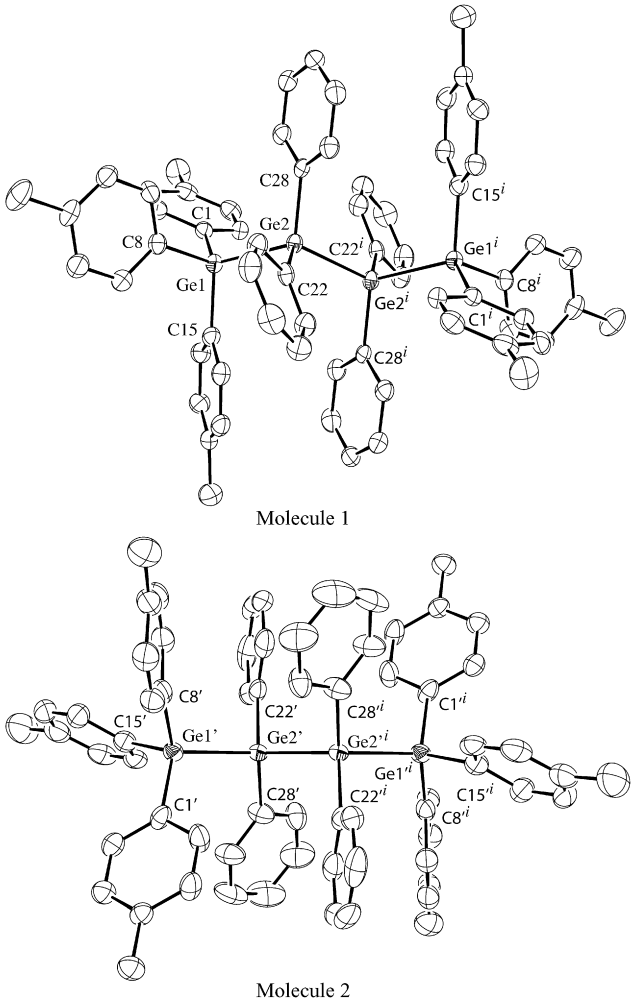

Fig. 4. ORTEP diagrams of the two crystallographically independent molecules of $Tol_3GeGePh_2GePh_2GeTol_3$ (**11**). Thermal ellipsoids are drawn at 50 % probability.

Table 4
Selected bond distances (Å) and angles (deg) for $Tol_3GeGePh_2GePh_2GeTol_3$ (**11**).

Molecule 1		Molecule 2[a]	
Ge(1)–Ge(2)	2.4490(8)	Ge(1′)–Ge(2′)	2.460(3)
Ge(2)–Ge(2^i)	2.457(1)	Ge(2′)–Ge(2′^{i})	2.448(3)
Ge(1)–C(1)	1.961(4)	Ge(1′)–C(1)	1.953(5)
Ge(1)–C(8)	1.960(4)	Ge(1′)–C(8)	2.008(5)
Ge(1)–C(15)	1.964(5)	Ge(1′)–C(15)	1.947(6)
Ge(2)–C(22)	1.971(4)	Ge(2′)–C(22)	1.980(5)
Ge(2)–C(28)	1.974(4)	Ge(2′)–C(28)	1.981(5)
Ge(1)–Ge(2)–Ge(2^i)	115.53(3)	Ge(1′)–Ge(2′)–Ge(2′^{i})	118.9(2)
C(1)–Ge(1)–C(8)	108.1(1)	C(1)–Ge(1′)–C(8)	106.6(2)
C(1)–Ge(1)–C(15)	107.5(2)	C(1)–Ge(1′)–C(15)	113.0(2)
C(8)–Ge(1)–C(15)	109.4(2)	C(8)–Ge(1′)–C(15)	106.8(2)
C(22)–Ge(2)–C(28)	106.2(2)	C(22)–Ge(2′)–C(28)	111.2(2)
C(1)–Ge(1)–Ge(2)	116.5(1)	C(1)–Ge(1′)–Ge(2′)	110.8(1)
C(8)–Ge(1)–Ge(2)	106.2(1)	C(8)–Ge(1′)–Ge(2′)	114.2(1)
C(15)–Ge(1)–Ge(2)	109.1(1)	C(15)–Ge(1′)–Ge(2′)	105.5(2)
C(22)–Ge(2)–Ge(1)	103.5(1)	C(22)–Ge(2′)–Ge(1′)	103.8(2)
C(28)–Ge(2)–Ge(1)	110.7(1)	C(28)–Ge(2′)–Ge(1′)	108.2(2)
C(22)–Ge(2)–Ge(2^i)	108.6(1)	C(22)–Ge(2′)–Ge(2′^{i})	107.8(1)
C(28)–Ge(2)–Ge(2^i)	111.5(1)	C(28)–Ge(2′)–Ge(2′^{i})	106.5(2)

[a] The germanium atoms in Molecule 2 of **11** are disordered over two positions with occupancies of 85.6 and 14.4%. Distances and angles including Ge(1′) and Ge (2′) are a weighted average based on the two occupancies.

Table 5
Torsion angles (deg) along the Ge(1)–Ge(2) and Ge(2)–Ge(2^i) bond in molecule 1 of $Tol_3GeGePh_2GePh_2GeTol_3$ (**11**).

C(1)–Ge(1)–Ge(2)–Ge(2^i)	72.8(1)	Ge(1)–Ge(2)–Ge(2^i)–C(22^i)	64.3(1)
C(1)–Ge(1)–Ge(2)–C(28)	55.1(1)	C(28)–Ge(2)–Ge(2^i)–C(22^i)	63.3(1)
C(8)–Ge(1)–Ge(2)–C(28)	65.3(1)	C(28)–Ge(2)–Ge(2^i)–Ge(1^i)	52.4(1)
C(8)–Ge(1)–Ge(2)–C(22)	48.2(1)	C(22)–Ge(2)–Ge(2^i)–Ge(1^i)	64.3(1)
C(15)–Ge(1)–Ge(2)–C(22)	69.6(1)	C(22)–Ge(2)–Ge(2^i)–C(28^i)	63.3(1)
C(15)–Ge(1)–Ge(2)–Ge(2^i)	49.0(1)	Ge(1)–Ge(2)–Ge(2^i)–C(28^i)	52.4(1)

effect on the Ge–Ge bond length as well as on the relative energies of the frontier molecular orbitals [42], and since tolyl substituents are more inductively electron-donating and also more sterically encumbering than phenyl substituents, the trends in both oxidation potential and Ge–Ge bond length are as expected.

Compounds **2** and **3** both exhibit two irreversible oxidation waves in their cyclic voltammograms. The first (least positive) oxidation wave was observed at 1498 ± 14 mV for **2** and 1542 ± 11 mV for **3**, while the second oxidation waves for **2** (1860 ± 15 mV) and **3** (1865 ± 13 mV) were observed at nearly identical potentials, and two oxidation waves were also observed for a sample of Ge_3Ph_8 at 1696 ± 12 mV and 2052 ± 15 mV. As found for the three digermanes described above, the same correlation of the potential of the first oxidation wave with bond length was observed for the trigermanes **2**, **3**, and Ge_3Ph_8. The Ge–Ge bond distances in **2** are 2.4318(5) and 2.4338(4) Å (av. 2.4328(5) Å) and are shorter the corresponding distances in **3**, which measure 2.4450(4) and 2.4395(5) Å (av. 2.4405(5) Å). The average Ge–Ge bond distance in Ge_3Ph_8 is similar to that of **3** and measures 2.440 (2) Å [39].

The data obtained for these digermanes and trigermanes suggests that decomposition of the oligogermane via germylene extrusion is occurring in these systems. The loss of $:GeR_2$ fragments has been detected via trapping with 2,3-dimethyl-1,3-butadiene from the photolysis of oligo [78] and polygermanes [79], and has also been postulated to occur in reactions of oligogermanes with tetracyanoethylene [77,80]. It should be noted, however, that homolytic Ge–Ge bond cleavage has also been observed as a competing process. The similarity of the potentials of the second oxidation waves in **2** and **3** suggests that the same chain contraction product is being generated from both molecules after the first oxidation event takes place. We propose that this species is $Ge_2Tol_6^{\bullet+}$, which is generated by the loss of $:GePh_2$ from **2** and $:GeTol_2$ from **3**. The oxidation potential for the digermane Ge_2Tol_6 (**1**) at 1757 ± 18 mV is also consistent with this statement, since the positively charged species $Ge_2Tol_6^{\bullet+}$ generated from **2** (1860 ± 15 mV) and **3** (1865 ± 13 mV) is expected to have a more positive oxidation potential than the neutral species **1**.

The first oxidation wave for Ge_3Ph_8 is at a more positive potential than that of both **2** and **3**, which is consistent with the observations for the three digermanes **1** and Ge_2Tol_6, and Ge_2Ph_6 described above. The first oxidation of Ge_3Ph_8 results in extrusion of $:GePh_2$ to generate $Ge_2Ph_6^{\bullet+}$ and this species undergoes an additional oxidation event at 2052 ± 15 mV, which is more positive

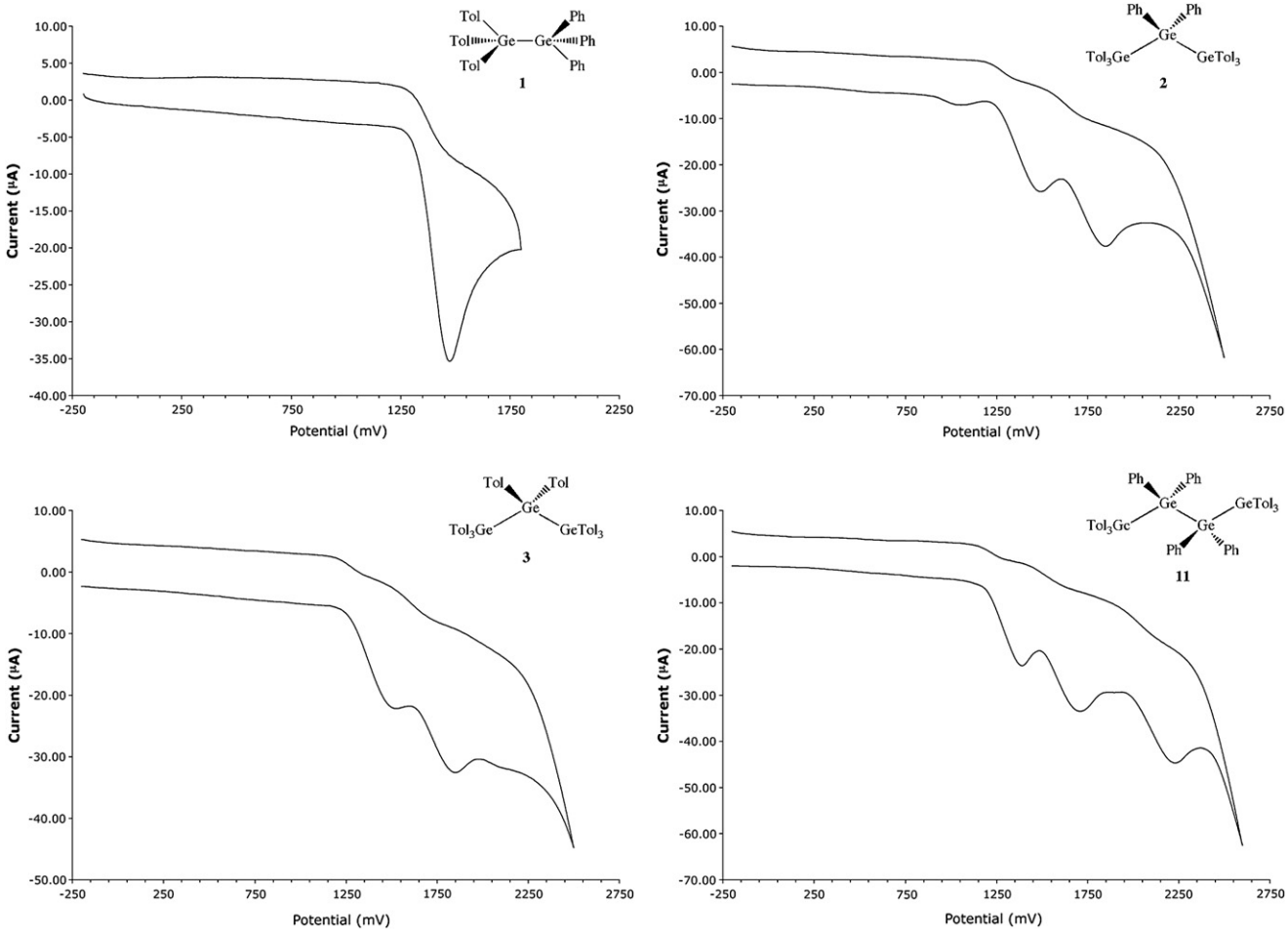

Fig. 5. Cyclic voltammograms for **1** – **3** and **11** in CH_2Cl_2 with 0.1M $[Bu_4N][PF_6]$ as the supporting electrolyte.

Table 6
Oxidation potentials, absorbance maxima and Ge–Ge bond distances for compounds **1**–**3**, **11**, Ge_2Tol_6 and Ge_nPh_{2n+2} ($n = 2$–4) in CH_2Cl_2 solution using 0.1 M $[Bu_4N][PF_6]$ as the supporting electrolyte.

Compound	E_{ox} (mV)	λ_{max} (nm)	d_{Ge-Ge} (Å)	Compound	E_{ox} (mV)	λ_{max} (nm)	d_{Ge-Ge} (Å)
$Tol_3GeGePh_3$ (**1**)	1483 ± 17	240	2.408(1)	Ge_2Tol_6	1757 ± 18	241	2.419(1)[b]
				Ge_2Ph_6 (**4**)	1958 ± 19	240	2.446(1)[c]
$Tol_3GeGePh_2GeTol_3$ (**2**)	1498 ± 14	251	2.4328(5)[a]	Ge_3Ph_8 (**6**)	1696 ± 12	238[d]	2.440(2)[d]
	1860 ± 15				2052 ± 15		
$Tol_3GeGeTol_2GeTol_3$ (**3**)	1542 ± 11	253	2.4405(5)[a]				
	1865 ± 13						
$Tol_3GeGePh_2GePh_2GeTol_3$ (**11**)	1398 ± 14	285	2.455(3)[a]	Ge_4Ph_{10} (**12**)	1644 ± 22	282[d]	2.462(2)[d]
	1718 ± 11				2060 ± 17		
	2242 ± 18				2450 ± 18		

[a] Average value.
[b] Data taken from ref. [48].
[c] Data taken from ref. [68].
[d] Data taken from ref. [39].

than the oxidation wave for the neutral compound Ge_2Ph_6 at 1958 ± 19 mV. The second oxidation wave for Ge_3Ph_8 also occurred at a more positive potential than that for both **2** and **3**, which is consistent with the oxidation wave of Ge_2Ph_6 being at a higher potential than both **1** and Ge_2Tol_6.

The CV for the tetragermane **11** exhibits three distinct waves at 1398 ± 14, 1718 ± 11, and 2242 ± 18 mV, indicating the sequential generation of two stable decomposition products. The CV of Ge_4Ph_{10} also exhibits three oxidation waves that each appear at more positive potentials (1644 ± 22, 2060 ± 17, and 2450 ± 18 mV)

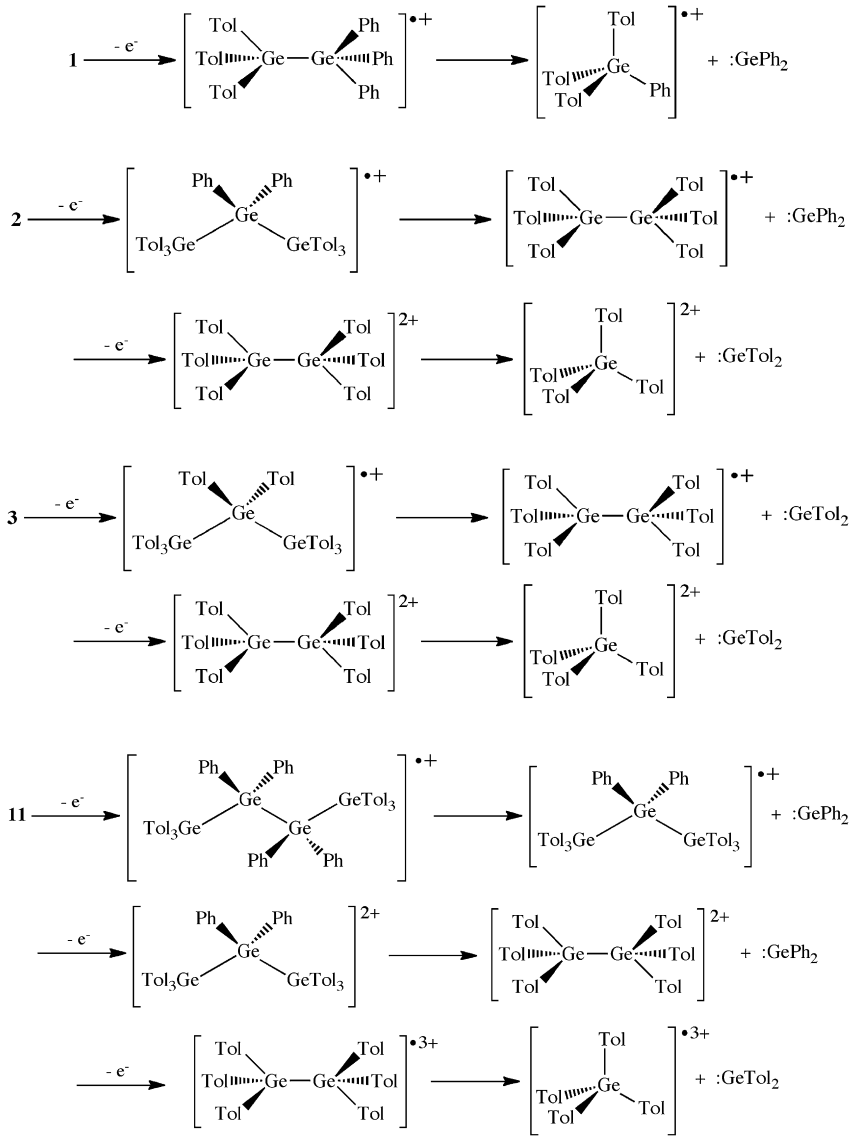

Scheme 3. Electrochemical decomposition pathways for **1** – **3** and **11**.

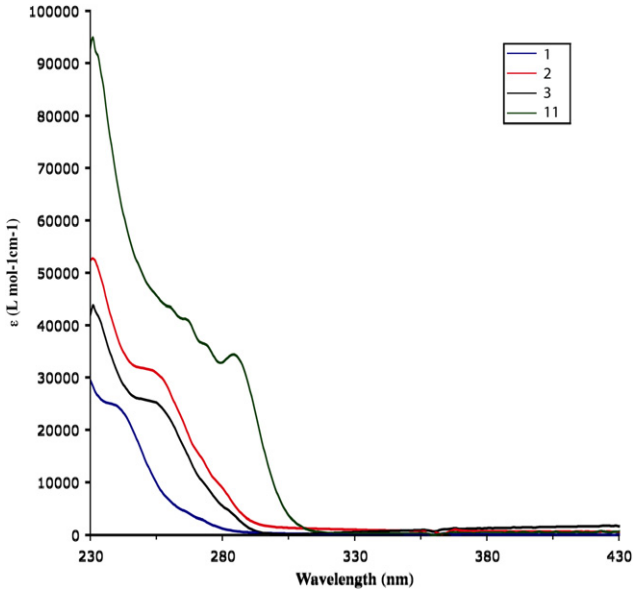

Fig. 6. UV/visible spectra of **1** – **3** and **11** in CH_2Cl_2 solution.

than the corresponding waves for **11**, which is again consistent with the results obtained for the phenyl-substituted digermanes and trigermanes versus their tolyl-containing analogs. The presence of three oxidation waves for **11** and Ge_4Ph_{10} suggest three germylene fragments are released from the Ge–Ge backbone, since this type of decomposition has been observed in photolysis studies of oligogermanes [77–80]. The first two germylenes resulting from the sequential oxidations of **11** are most likely :$GePh_2$, since the internal germanium atoms are phenyl substituted and are more susceptible to elimination. In the perphenyl-substituted tetragermane Ge_4Ph_{10}, all three of the germylenes released are: $GePh_2$, but the third oxidation of **11** results in the generation of the radical trivalent cation $Tol_3GeGeTol_3^{\bullet 3+}$, and this species then subsequently decomposes via elimination of the germylene :$GeTol_2$.

The UV/visible spectra of **1**–**3** and **11** are shown in Fig. 6 and the λ_{max} values are collected in Table 6. The expected trend among the di, tri, and tetragermanes was observed, where the position of λ_{max} is red shifted with increasing catenation. The absorbance maximum corresponding to the $\sigma \rightarrow \sigma^*$ transition in the tetragermane **11** at 285 nm (ε 3.43×10^4 L mol^{-1} cm^{-1}) is at lower energy than those of the trigermanes **2** and **3** and the digermane **1**. In addition to the band at 285 nm, three additional features at 274, 268, and 260 nm are present in the UV/visible spectrum of **11**, which are assigned to electronic transitions between the π and π^* orbitals of the aryl ligands. Similar $\pi \rightarrow \pi^*$ transitions for compounds **1**–**3** also are likely to occur, but the peaks for these transitions were not visible due to their overlap with the intense λ_{max} feature resulting from the $\sigma \rightarrow \sigma^*$ electronic transition. The red shift of the λ_{max} for **11** versus those for **1**–**3** allows these additional absorbance features to be observed in **11**. The λ_{max} for Ge_4Ph_{10} was reported at 282 nm (ε 3.98×10^4 L mol^{-1} cm^{-1}), and a second defined feature was also observed at 228 nm [39]. The λ_{max} for **2** (251 nm, ε

Table 7
Crystal data and structure refinement details for **1**·$2C_6H_6$, **2**·C_7H_8, **3**·C_7H_8, and **11**.

Compound	**1**·$2C_6H_6$	**2**·C_7H_8	**3**·C_7H_8	**11**
Empirical formula	$C_{51}H_{48}Ge_2$	$C_{61}H_{60}Ge_3$	$C_{63}H_{64}Ge_3$	$C_{66}H_{62}Ge_4$
Temperature (K)	150(2)	120(2)	150(2)	150(2)
Wavelength (Å)	0.71073	0.71073	0.71073	0.71073
Crystal system	Triclinic	Monoclinic	Triclinic	Triclinic
Space group	$P-1$	$P2_1/n$	$P-1$	$P-1$
a (Å)	8.884(5)	13.7610(5)	11.563(2)	11.582(4)
b (Å)	10.428(6)	26.044(1)	13.825(2)	13.114(4)
c (Å)	21.52(1)	14.1583(5)	17.739(3)	19.527(6)
α (°)	89.200(8)	90	86.381(2)	83.531(5)
β (°)	79.094(8)	92.437(2)	88.798(2)	79.175(4)
γ (°)	81.806(8)	90	72.552(2)	72.021(4)
Volume (Å^3)	1937(2)	5069.6(3)	2702.3(8)	2766(1)
Z, Z'	2,0	4,0	2,0	2,0
Calculated density (g/cm^3)	1.315	1.324	1.277	1.375
Absorption coefficient (mm^{-1})	1.584	2.374	1.695	2.192
F(000)	794	2088	1076	1172
Crystal size (mm)	0.25 × 0.18 × 0.12	0.15 × 0.10 × 0.10	0.35 × 0.15 × 0.08	0.25 × 0.21 × 0.11
Crystal size and shape	Colorless block	Colorless block	Colorless block	Colorless block
θ range for data collection (o)	1.93–28.31	3.39–66.11	1.55–28.20	1.64–27.51
Index ranges	$-11 \le h \le 11$	$-15 \le h \le 13$	$-15 \le h \le 15$	$-12 \le h \le 14$
	$-13 \le k \le 13$	$-28 \le k \le 29$	$-17 \le k \le 18$	$-12 \le k \le 16$
	$-28 \le l \le 28$	$-14 \le l \le 16$	$-23 \le l \le 23$	$-25 \le l \le 24$
Reflections collected	42 366	26 445	69 956	15 530
Independent reflections	9055 (R_{int} = 0.0456)	8224 (R_{int} = 0.0502)	12 152 (R_{int} = 0.0431)	9778 (R_{int} = 0.0335)
Completeness to θ	25.00 (99.9%)	60.00 (99.4%)	25.00 (99.8%)	25.00 (83.2%)
Absorption correction	Multi-scan	Multi-scan	Multi-scan	Multi-scan
Maximum and minimum transmission	0.8327 and 0.6929	0.7972 and 0.7171	0.8763 and 0.5884	0.7945 and 0.6102
Refinement method	Full-matrix least-squares on F^2	Full-matrix least-squares on F^2	Full-matrix least-squares on F^2	Full-matrix least-squares on F^2
Data/restraints/parameters	9055/0/454	8224/0/520	12152/0/540	9778/0/656
Goodness of fit on F^2	1.053	1.032	1.075	1.026
Final R indices ($I > 2\sigma(I)$)				
R_1	0.0320	0.0367	0.0374	0.0499
wR_2	0.0701	0.0773	0.0915	0.1110
Final R indices (all data)				
R_1	0.0534	0.0544	0.0448	0.0691
wR_2	0.0750	0.0813	0.0968	0.1237
Largest difference in peak and hole (e Å^{-3})	0.433 and −0.295	0.591 and −0.347	1.070 and −0.666	0.808 and −0.487

3.17×10^4 L mol^{-1} cm^{-1}) and **3** (253 nm, ε 2.55×10^4 L mol^{-1} cm^{-1}) appear at nearly the same wavelength, and are red shifted relative to that of **1** but are blue shifted relative to that of **11**. Both absorbance maxima are red shifted relative to the reported λ_{max} for Ge_3Ph_8 at 238 nm (ε 3.16×10^4 L mol^{-1} cm^{-1}) [39]; however, the λ_{max} for **1** and $Ge_2Ph_{6[36]}$ were both observed at 240 nm.

3. Conclusions

The series of *para*-tolyl-substituted oligogermanes $Tol_3GeGePh_3$ (**1**), $Tol_3GeGePh_2GeTol_3$ (**2**), $Tol_3GeGeTol_2GeTol_3$ (**3**), and $Tol_3GeGePh_2GePh_2GeTol_3$ (**11**) can be prepared via the hydrogermolysis reaction using Tol_3GeNMe_2 and Tol_2GeH_2 as synthetic building blocks. The structures of these four compounds differ from their *per*-phenyl-substituted analogs, in both the Ge–Ge bond distances and, in the case of **2**, **3** and **11**, in the Ge–Ge–Ge bond angles, due to the different steric and electronic effects of the tolyl substituents. In general, the Ge–Ge bond distances are shorter and the Ge–Ge–Ge bond angles are more acute when tolyl substituents are introduced along the Ge–Ge backbone in place of phenyl substituents.

The incorporation of tolyl substituents also has an effect on the oxidation potential and UV/visible absorbance maxima in these compounds. Oligogermanes **1**–**3** and **11**, which have the general formula Ge_nAr_{2n+2} (Ar = *p*-$CH_3C_6H_4$ or Ph), exhibit $n - 1$ oxidation waves in their cyclic voltammograms. This has not been observed previously, as oligogermanes typically exhibit only one irreversible oxidation wave regardless of the degree of catenation. We suggest that the first oxidation event for **1**–**3** results in extrusion of the germylene :$GeTol_2$, and the resulting electrochemical by-products for **2** and **3** are stable and undergo a second oxidation event with concomitant extrusion of a second germylene fragment.

4. Experimental section

4.1. General considerations

All manipulations were performed under an atmosphere of nitrogen using standard Schlenk, syringe, and glovebox techniques [81]. The reagents *p*-$CH_3C_6H_4Cl$, elemental Mg, TolMgBr (1.0 M solution in THF), Ph_3GeH, $LiNMe_2$, trichloroacetic acid, and $LiAlH_4$ were purchased from Aldrich. The compounds $GeBr_4$, $GeCl_4$, and Ge_2Ph_6 were purchased from Gelest, Inc. Solvents were purified using a Glass Contour Solvent Purification System. NMR spectra were recorded in C_6D_6 at room temperature using a Varian Gemini 2000 spectrometer operating at 300 MHz (^{1}H) or 75.5 MHz (^{13}C) and were referenced to the C_6D_6 solvent. Cyclic voltammograms were obtained using a Bioanalytical Systems Epsilon Electrochemical Workstation with a glassy-carbon working electrode, a platinum wire counter electrode, and an Ag/AgCl reference electrode using 1.0 M [Bu_4N][PF_6] as the supporting electrolyte. UV/visible spectra were obtained using a Hewlett–Packard Agilent UV/visible spectroscopy system. IR spectra were recorded using a Hewlett–Packard Infrared Spectrometer. Elemental analyses were obtained by Midwest Microlabs or Galbraith Laboratories.

4.2. Synthesis of Tol_3GeCl

A flame-dried 3-necked flask equipped with a reflux condenser was charged with magnesium metal (4.30 g, 177 mmol). A solution of *p*-$CH_3C_6H_4Cl$ (14.92 g, 117.9 mmol) in THF (100 mL) was placed in a dropping funnel. The magnesium metal was coated with approx. 15 mL of the *p*-$CH_3C_6H_4Cl$ solution and a crystal of iodine was added to the flask. The mixture was gently heated with a heat gun until the iodine color had faded, and the remaining *p*-$CH_3C_6H_4Cl$ solution was added dropwise over 45 min. The resulting reaction mixture was refluxed for 2 h, was allowed to cool, and then was added to a solution of $GeCl_4$ (8.43 g, 39.3 mmol) in THF (50 mL). The reaction mixture was refluxed for 90 min, was allowed to cool, and then was carefully poured over a 20% aqueous HCl solution at 0 °C. The THF layer was separated and the aqueous layer was extracted with ether (3 × 50 mL). The combined THF layer and ethereal extracts were dried over anhydrous $MgSO_4$. The suspension was filtered and the volatiles were removed *in vacuo* to yield a viscous oil. The crude product was distilled *in vacuo* (125 °C, 0.05 torr) to remove impurities to yield Tol_3GeCl (12.425 g, 83%) as a white solid. ^{1}H NMR δ 7.66 (d, $J = 7.8$ Hz, 6H, *o*-$H_3CC_6H_4$), 7.00 (d, $J = 7.8$ Hz, 6H, *m*-$H_3CC_6H_4$), 2.06 (s, 9H, $H_3CC_6H_4$) ppm. ^{13}C NMR δ 140.6 (*ipso*-$H_3CC_6H_4$), 134.6 (*o*-$H_3CC_6H_4$), 130.0 (*p*-$H_3CC_6H_5$), 129.8 (*m*-$H_3CC_6H_4$), 21.4 (*p*-$H_3CC_6H_4$) ppm. Anal. Calcd. for $C_{21}H_{21}ClGe$: C, 66.10; H, 5.55. Found: C, 66.25; H, 5.61.

4.3. Synthesis of Tol_3GeNMe_2

To a solution of Tol_3GeCl (1.951 g, 5.117 mmol) in benzene (20 mL) was added a suspension of $LiNMe_2$ (0.280 g, 5.49 mmol) in benzene (10 mL). The reaction mixture was stirred for 18 h and then filtered through Celite. The volatiles were removed *in vacuo* to yield Tol_3GeNMe_2 (1.51 g, 76%) as a thick colorless oil. ^{1}H NMR δ 7.71 (d, $J = 7.8$ Hz, 6H, *o*-$H_3CC_6H_4$), 7.09 (d, $J = 7.8$ Hz, 6H, *m*-$H_3CC_6H_4$), 2.84 (s, 6H, $N(CH_3)_2$), 2.11 (s, 9H, $H_3CC_6H_4$) ppm. ^{13}C NMR δ 139.1 (*ipso*-$H_3CC_6H_4$), 135.5 (*o*-$H_3CC_6H_4$), 129.4 (*p*-$H_3CC_6H_5$), 129.4 (*m*-$H_3CC_6H_4$), 41.7 ($N(CH_3)_2$), 21.4 (*p*-$H_3CC_6H_4$) ppm. Anal. Calcd. for $C_{23}H_{27}GeN$: C, 70.80; H, 6.98. Found: C, 71.21; H, 7.08.

4.4. Synthesis of Tol_2GeBr_2 [82] and Tol_2GeH_2 [83]

To a solution of $GeBr_4$ (5.00 g, 12.7 mmol) at 0 °C in ether (70 mL) was added a solution of TolMgBr in THF (1.0 M, 25.5 mL) dropwise via syringe. The resulting reaction mixture was refluxed for 3 h, was allowed to cool, and was carefully poured over a 0.1 M aqueous HBr solution. The aqueous layer was separated and extracted with ether (3 × 25 mL). The organic layer and the combined ether extracts were dried over anhydrous $MgSO_4$. The volatiles were removed *in vacuo* after filtration to yield a viscous liquid. The crude reaction mixture (1.852 g) in ether (30 mL) was treated with a suspension of $LiAlH_4$ (0.340 g, 8.94 mmol) in ether (30 mL) at 0 °C. The reaction mixture was subsequently refluxed for 3 h and then was quenched with 1 M aqueous HCl at −78 °C. The temperature was raised to 25 °C and the reaction mixture was stirred for 30 min. The solution was cooled to −78 °C and the ether layer was cannulated into a separate flask. The remaining aqueous layer was extracted with ether (2 × 15 mL) and the combined ether solutions were dried over anhydrous $MgSO_4$. The volatiles were removed *in vacuo* to yield a colorless liquid that was distilled *in vacuo* (65 °C, 0.10 torr) to yield Tol_2GeH_2 (0.250 g, 8% based on $GeBr_4$). ^{1}H NMR δ 7.43 (d, $J = 7.5$ Hz, 4H, *o*-$H_3CC_6H_4$), 6.99 (d, $J = 7.5$ Hz, 4H, *m*-$H_3CC_6H_4$), 5.22 (s, 2H, Ge*H*), 2.07 (s, 6H, $H_3CC_6H_4$) ppm. ^{13}C NMR δ 139.8 (*ipso*-$H_3CC_6H_4$), 136.5 (*o*-$H_3CC_6H_4$), 131.7 (*p*-$H_3CC_6H_4$), 130.6 (*m*-$H_3CC_6H_4$), 22.4 (*p*-$H_3CC_6H_4$) ppm. Anal. Calcd. for $C_{14}H_{16}Ge$: C, 65.43; H, 6.28. Found: C, 65.22; H, 6.37.

4.5. Synthesis of $Tol_3GeGePh_3$ (**1**)

To a solution of Ph_3GeH (0.380 g, 1.25 mmol) in CH_3CN (10 mL) was added a solution of Tol_3GeNMe_2 (0.484 g, 1.24 mmol) in CH_3CN (10 mL). The reaction mixture was sealed in a Schlenk tube and stirred for 48 h at 90 °C. The volatiles were removed *in vacuo* to yield an off-white solid. Distillation in a Kugelrohr oven (125 °C, 0.050 torr) to remove excess Ph_3GeH yielded a white solid that was recrystallized from a hot benzene (5 mL) solution to yield **1** as

colorless crystals (0.684 g, 85%). ^{1}H NMR δ 7.68–7.64 (m, 9H, *m*-C_6H_5 and *p*-C_6H_5), 7.57 (d, J = 7.5 Hz, 6H, *o*-$H_3CC_6H_4$), 7.10 (m, 6H, *o*-C_6H_5), 6.93 (d, J = 7.5 Hz, 6H, *m*-$H_3CC_6H_4$), 2.02 (s, 9H, $H_3CC_6H_4$) ppm. ^{13}C NMR δ 138.8 (*ipso*-$H_3CC_6H_4$), 136.2 (*o*-$H_3CC_6H_4$), 136.0 (*o*-C_6H_5), 133.6 (*ipso*-C_6H_5), 129.7 (*p*-C_6H_5), 129.2 (*p*-$H_3CC_6H_4$), 128.8 (*m*-$H_3CC_6H_4$), 127.7 (*m*-C_6H_5), 21.4 (*p*-$H_3CC_6H_4$) ppm. Anal. Calcd. for $C_{51}H_{48}Ge_2$ (**1**·2C_6H_6): C, 75.96; H, 6.00. Found: C, 75.81; H, 6.11.

4.6. Synthesis of $Tol_3GeGePh_2GeTol_3$ (**2**)

To a solution of Ph_2GeH_2 (0.100 g, 0.437 mmol) in acetonitrile (10 mL) in a Schlenk tube was added a solution of Tol_3GeNMe_2 (0.340 g, 0.874 mmol) in acetonitrile (10 mL). The tube was sealed and the reaction mixture was stirred in an oil bath at 90 °C for 48 h. The volatiles were removed *in vacuo* to yield a white solid that was distilled in a Kugelrohr oven (125 °C, 0.05 torr). The material remaining in the distillation flask was recrystallized from hot toluene to yield **2** (0.283 g, 71%) as colorless crystals. ^{1}H NMR δ 7.78–7.74 (m, 6H, *m*-C_6H_5 and *p*-C_6H_5), 7.46 (d, J = 7.5 Hz, 12H, *o*-$H_3CC_6H_4$), 7.05–7.03 (m, 4H, *o*-C_6H_5), 6.91 (d, J = 7.5 Hz, 12H, *m*-$H_3CC_6H_4$), 2.07 (s, 18H, $H_3CC_6H_4$) ppm. ^{13}C NMR δ 139.1 (*ipso*-$H_3CC_6H_4$), 137.0 (*o*-$H_3CC_6H_4$), 136.2 (*o*-C_6H_5), 134.9 (*ipso*-C_6H_5), 129.4 (*p*-C_6H_5), 128.6 (*p*-$H_3CC_6H_4$), 128.3 (*m*-$H_3CC_6H_4$), 127.9 (*m*-C_6H_5), 21.3 (*p*-$H_3CC_6H_4$) ppm. Anal. Calcd. for $C_{61}H_{60}Ge_3$ (**2**·C_7H_8): C, 72.45; H, 5.98. Found: C, 72.39; H, 6.01.

4.7. Synthesis of $Tol_3GeGeTol_2GeTol_3$ (**3**)

To a solution of Tol_2GeH_2 (0.175 g, 0.681 mmol) in acetonitrile (10 mL) in a Schlenk tube was added a solution of Tol_3GeNMe_2 (0.531 g, 1.36 mmol) in acetonitrile (10 mL). The tube was sealed and the reaction mixture was stirred in an oil bath at 90 °C for 48 h. The volatiles were removed *in vacuo* to yield a pale yellow solid that was recrystallized from a hot benzene/hexane mixture (1:1, 10 mL) to yield **3** (0.458 g, 71%) as colorless crystals. ^{1}H NMR δ 7.69 (d, J = 7.8 Hz, 4H, *o*-Ge($C_6H_4CH_3)_2$), 7.49 (d, J = 7.8 Hz, 12H, *o*-Ge($C_6H_4CH_3)_3$), 6.93 (d, J = 7.8 Hz, 12H, *m*-Ge($C_6H_4CH_3)_3$), 6.87 (d, J = 7.8 Hz, 4H, *m*-Ge($C_6H_4CH_3)_2$), 2.09 (s, 18H, Ge($C_6H_4CH_3)_3$), 1.99 (s, 6H, Ge($C_6H_4CH_3)_2$) ppm. ^{13}C NMR δ 138.3 (*ipso*-Ge($C_6H_4CH_3)_3$), 138.2 (*ipso*-Ge($C_6H_4CH_3)_2$), 137.0 (*o*-Ge($C_6H_4CH_3)_2$), 136.4 (*o*-Ge($C_6H_4CH_3)_3$), 135.4 (*p*-Ge($C_6H_4CH_3)_2$), 135.2 (*p*-Ge($C_6H_4CH_3)_3$), 129.4 (*m*-Ge($C_6H_4CH_3)_3$), 129.3 (*m*-Ge($C_6H_4CH_3)_2$), 21.4 (Ge($C_6H_4CH_3)_3$), 21.3 (Ge($C_6H_4CH_3)_2$) ppm. Anal. Calcd. for $C_{56}H_{56}Ge_3$ (**3**): C, 71.01; H, 5.96. Found: C, 70.91; H, 5.96.

4.8. Synthesis of $Cl_3(O)COPh_2GeGePh_2OC(O)CCl_3$ (**5**) [51]

To a solution of $Ph_3GeGePh_3$ (2.000 g, 3.392 mmol) in toluene (3.6 mL) was added a solution of $Cl_3CC(O)OH$ (2.34 g, 14.32 mmol) in toluene (3.0 mL). The reaction mixture sealed in a Schlenk tube and was heated at 110 °C for 72 h in an oil bath. The resulting solution was cooled to room temperature and layered with hexane to yield a white precipitate which was filtered and washed with a mixture of hexane and toluene (1:1) to yield **5** (2.006 g, 76%) as a white solid. IR (Nujol mull): 1644.8 cm^{-1} (ν_{CO}).

4.9. Synthesis of $ClPh_2GeGePh_2Cl$ (**8**) [51]

To a solution of **5** (1.050 g, 1.349 mmol) in acetone (8.75 mL) was added 3 ml of concentrated hydrochloric acid. The reaction mixture was stirred under N_2 at 50 °C for 18 h in an oil bath. The resulting dark red solution was cooled to −28 °C using a dry ice/*ortho*-xylene mixture to yield ochre-colored crystals which were washed with a mixture of hexane and acetone (1:1). Recrystallization of the crude product with a mixture of E_2O and hexane (2:1) yielded **8** (0.382 g, 54%) as needle-shaped colorless crystals. ^{1}H NMR δ 7.77–7.73 (m, 8H, *o*-C_6H_5), 7.03–7.01 (m, 12H, *m*-C_6H_5 and *p*-C_6H_5) ppm. ^{13}C NMR δ 136.0 (*ipso*-C_6H_5), 134.1 (*o*-C_6H_5), 130.8 (*p*-C_6H_5), 129.1 (*m*-C_6H_5) ppm.

4.10. Synthesis of $HPh_2GeGePh_2H$ (**10**)

To a solution of **8** (0.110 g, 0.209 mmol) in THF (10 mL) was added a suspension of $LiAlH_4$ (0.016 g, 0.416 mmol) in THF (10 mL). The resulting mixture was stirred for 18 h under N_2. The solvent was removed *in vacuo* yielding a white solid that was washed with benzene (2 × 3 mL). The product was dried *in vacuo* to yield **10** (0.075 g, 79%) as a white solid. ^{1}H NMR δ 7.54–7.50 (m, 8H, *o*-C_6H_5), 7.08–7.04 (m, 12H, *m*-C_6H_5 and *p*-C_6H_5), 5.58 (s, 2H, Ge*H*) ppm. ^{13}C NMR δ 136.0 (*ipso*-C_6H_5), 135.7 (*o*-C_6H_5), 129.1 (*p*-C_6H_5), 128.7 (*m*-C_6H_5) ppm. IR (Nujol mull): 2033 cm^{-1}.

4.11. Synthesis of $Tol_3GeGePh_2GePh_2GeTol_3$ (**11**)

To a solution of **10** (0.075 g, 0.165 mmol) in acetonitrile (5 mL) in a Schlenk tube was added a solution of Tol_3GeNMe_2 (0.128 g, 0.330 mmol) in CH3CN (5 mL). The tube was sealed and the reaction mixture was stirred in an oil bath at 90 °C for 48 h. The volatiles were removed *in vacuo* to yield a pale yellow solid that was recrystallized from a hot benzene/hexane mixture (1:1, 10 mL) to yield **11** (0.150 g, 80%) as colorless crystals. ^{1}H NMR δ 7.55 (d, J = 7.5 Hz, 12H, *o*-$C_6H_4CH_3$), 7.31 (d, J = 7.2 Hz, 8H, *o*-C_6H_5), 7.11 (t, J = 7.2 Hz, 4H, *p*-C_6H_5), 6.97 (t, J = 7.2 Hz, 8H, *m*-C_6H_5), 6.85 (d, J = 7.5 Hz, 12H, *m*-$C_6H_4CH_3$), 2.02 (s, 18H, $C_6H_4CH_3$) ppm. ^{13}C NMR δ 138.4 (*ipso*-$H_3CC_6H_4$), 137.2 (*o*-C_6H_5), 136.2 (*o*-$CH_3C_6H_4$), 135.1 (*ipso*-C_6H_5), 129.5 (*p*-C_6H_5), 129.4 (*p*-$H_3CC_6H_4$), 128.4 (*m*-$H_3CC_6H_4$), 127.9 (*m*-C_6H_5), 21.3 (*p*-$H_3CC_6H_4$) ppm. Anal. Calcd. for $C_{80}H_{78}Ge_4$ (**7**·2C_7H_8): C, 72.23; H, 5.91. Found: C, 72.38; H, 6.05.

4.12. X-ray crystal structure of compounds **1**–**3** and **11**

Diffraction intensity data were collected with a Siemens P4/CCD diffractometer. Crystallographic data and details are shown in Table 7. Absorption corrections were applied for all data using SADABS. The structures were solved using direct methods, completed by difference Fourier syntheses, and refined on full-matrix least-squares procedures on F^2. All ordered non-hydrogen atoms were refined with anisotroptic displacement coefficients and hydrogen atoms were treated as idealized contributions. Solvent molecules were removed using SQUEEZE for compounds **2** and **3**. All software and sources of scattering factors are contained in the SHEXTL (5.10) program package (G. Sheldrick, Bruker XRD, Madison, WI). ORTEP diagrams were drawn using the ORTEP3 program (L.J. Farrugia, Glasgow).

Acknowledgment

Funding for this work by a CAREER award from the National Science Foundation (Grant CHE-0844758) is gratefully acknowledged.

Appendix A. Supplementary material

CCDC 763304 (**1**), 763305 (**2**), 763306 (**3**), 763308 (**11**) contain supplementary crystallographic data. These data can be obtained free of charge from the Cambridge Crystallographic Data Center via www.ccdc.cam.ac.uk/data_request/cif.

References

[1] V. Balaji, J. Michl, Polyhedron 10 (1991) 1265–1284.
[2] R.D. Miller, J. Michl, Chem. Rev. 89 (1989) 1359–1410.
[3] J.V. Ortiz, Polyhedron 10 (1991) 1285–1297.
[4] L.R. Sita, Acc. Chem. Res. 27 (1994) 191–197.
[5] L.R. Sita, Adv. Organomet. Chem. 38 (1995) 189–243.
[6] M.L. Amadoruge, C.S. Weinert, Chem. Rev. 108 (2008) 4253–4294.
[7] C.S. Weinert, Dalton Trans. (2009) 1691–1699.
[8] M. Dräger, L. Ross, D. Simon, Rev. Silicon Germanium Tin Lead Compd. 7 (1983) 299–445.
[9] R.E. Benfield, R.H. Cragg, R.G. Jones, A.C. Swain, J. Chem. Soc. Chem. Commun. (1992) 1022–1024.
[10] D. Bratton, S.J. Holder, R.G. Jones, W.K.C. Wong, J. Organomet. Chem. 685 (2003) 60–64.
[11] E.F. Hengge, J. Inorg. Organomet. Polym. 3 (1993) 287–303.
[12] R.G. Jones, R.E. Benfield, R.H. Cragg, A.C. Swain, S.J. Webb, Macromolecules 26 (1993) 4878–4887.
[13] S. Kashimura, M. Ishifune, N. Yamashita, H.-B. Bu, M. Takebayashi, S. Kitajima, D. Yoshiwara, Y. Kataoka, R. Nishida, S. Kawasaki, H. Murase, T. Shono, J. Org. Chem. 64 (1999) 6615–6621.
[14] Y. Kimata, H. Suzuki, S. Satoh, A. Kuriyama, Chem. Lett. (1994) 1163–1164.
[15] Y. Kimata, H. Suzuki, S. Satoh, A. Kuriyama, Organometallics 14 (1995) 2506–2511.
[16] B. Lacave-Goffin, L. Hevesi, J. Devaux, J. Chem. Soc. Chem. Commun. (1995) 769–770.
[17] R.D. Miller, P.K. Jenkner, Macromolecules 27 (1994) 5921–5923.
[18] R. Shankar, A. Saxena, A.S. Brar, J. Organomet. Chem. 650 (2002) 223–230.
[19] V.V. Zuev, N.K. Skvortsov, J. Polym. Sci. A: Polym. Chem. 41 (2003) 3761–3767.
[20] S. Adams, M. Dräger, J. Organomet. Chem. 288 (1985) 295–304.
[21] S. Adams, M. Dräger, B. Mathiasch, J. Organomet. Chem. 326 (1987) 173–186.
[22] J.R. Babcock, L.R. Sita, J. Am. Chem. Soc. 118 (1996) 12481–12482.
[23] F. Choffat, P. Smith, W. Caseri, J. Mater. Chem. 15 (2005) 1789–1792.
[24] P.R. Deacon, N. Devylder, M.S. Hill, M.F. Mahon, K.C. Molloy, G.J. Price, J. Organomet. Chem. 687 (2003) 46–56.
[25] S.J. Holder, R.G. Jones, R.E. Benfield, M.J. Went, Polymer 37 (1996) 3477–3479.
[26] T. Imori, V. Lu, H. Cai, T.D. Tilley, J. Am. Chem. Soc. 117 (1995) 9931–9940.
[27] T. Imori, T.D. Tilley, J. Chem. Soc. Chem. Commun. (1993) 1607–1609.
[28] V. Lu, T.D. Tilley, Macromolecules 29 (1996) 5763–5764.
[29] V.Y. Lu, T.D. Tilley, Macromolecules 33 (2000) 2403–2412.
[30] K. Mochida, M. Hayakawa, T. Tsuchikawa, Y. Yokoyama, M. Wakasa, H. Hayashi, Chem. Lett. (1998) 91–92.
[31] M. Okano, N. Matsumoto, M. Arakawa, T. Tsuruta, H. Hamano, Chem. Commun. (1998) 1799–1800.
[32] L.R. Sita, Organometallics 11 (1992) 1442–1444.
[33] L.R. Sita, K.W. Terry, K. Shibata, J. Am. Chem. Soc. 117 (1995) 8049–8050.
[34] R. Sommer, B. Schneider, W.P. Neumann, Justus Liebigs Ann. Chem. 692 (1966) 12–21.
[35] S.M. Thompson, U. Schubert, Inorg. Chim. Acta 357 (2004) 1959–1964.
[36] A. Castel, P. Rivière, B. Saint-Roch, J. Satgé, J.P. Malrieu, J. Organomet. Chem. 247 (1983) 149–160.
[37] W.P. Neumann, K. Kühlein, Tetrahedron Lett. (1963) 1541–1545.
[38] W.P. Neumann, K. Kühlein, Liebigs Ann. Chem. 683 (1965) 1–11.
[39] S. Roller, D. Simon, M. Dräger, J. Organomet. Chem. 301 (1986) 27–40.
[40] K. Triplett, M.D. Curtis, J. Organomet. Chem. 107 (1976) 23–32.
[41] M.L. Amadoruge, A.G. DiPasquale, A.L. Rheingold, C.S. Weinert, J. Organomet. Chem. 693 (2008) 1771–1778.
[42] M.L. Amadoruge, J.R. Gardinier, C.S. Weinert, Organometallics 27 (2008) 3753–3760.
[43] M.L. Amadoruge, J.A. Golen, A.L. Rheingold, C.S. Weinert, Organometallics 27 (2008) 1979–1984.
[44] M.L. Amadoruge, C.H. Yoder, J.H. Conneywerdy, K. Heroux, A.L. Rheingold, C. S. Weinert, Organometallics 28 (2009) 3067–3073.
[45] E. Subashi, A.L. Rheingold, C.S. Weinert, Organometallics 25 (2006) 3211–3219.
[46] K. Mochida, C. Hodota, R. Hata, S. Fukuzumi, Organometallics 12 (1993) 586–588.
[47] M. Okano, K. Mochida, Chem. Lett. (1990) 701–704.
[48] M. Dräger, L. Ross, Z. Anorg. Allg. Chem. 469 (1980) 115–122.
[49] L. Párkányi, A. Kálmán, S. Sharma, D.M. Nolen, K.H. Pannell, Inorg. Chem. 33 (1994) 180–182.
[50] S. Roller, M. Dräger, J. Organomet. Chem. 316 (1986) 57–65.
[51] D. Simon, K. Häberle, M. Dräger, J. Organomet. Chem. 267 (1984) 133–142.
[52] M. Dräger, L. Ross, Z. Anorg. Allg. Chem. 460 (1980) 207–216.
[53] H. Puff, H. Heisig, W. Schuh, W. Schwab, J. Organomet. Chem. 303 (1986) 343–350.
[54] H. Puff, T.R. Kök, P. Nauroth, W. Schuh, J. Organomet. Chem. 281 (1985) 141–148.
[55] K. Häberle, M. Dräger, Z. Naturforsch 42B (1987) 323–329.
[56] M. Dräger, K. Häberle, J. Organomet. Chem. 280 (1985) 183–196.
[57] Y. Liu, D. Ballweg, T. Müller, I.A. Guzei, R.W. Clark, R. West, J. Am. Chem. Soc. 124 (2002) 12174–12181.
[58] G.H. Spikes, J.C. Fettinger, P.P. Power, J. Am. Chem. Soc. 127 (2005) 12232–12233.
[59] H. Schäfer, W. Saak, M. Weidenbruch, J. Organomet. Chem. 604 (2000) 211–213.
[60] W. Setaka, K. Sakamoto, M. Kira, P.P. Power, Organometallics 20 (2001) 4460–4462.
[61] J. Baumgartner, R. Fischer, J. Fischer, A. Wallner, C. Marschner, U. Flörke, Organometallics 24 (2005) 6450–6457.
[62] S.P. Mallela, R.A. Geanangel, Inorg. Chem. 30 (1991) 1480–1482.
[63] M. Weidenbruch, F.-T. Grimm, M. Herrndorf, A. Schäfer, K. Peters, H.G. von Schnering, J. Organomet. Chem. 341 (1988) 335–343.
[64] J.E. Bender IV, M.M. Banaszak Holl, A. Mitchell, N.J. Wells, J.W. Kampf, Organometallics 17 (1998) 5166–5171.
[65] J.E. Bender IV, K.E. Litz, D. Giarikos, N.J. Wells, M.M. Banaszak Holl, J.W. Kampf, Chem. Eur. J. 3 (1997) 1793–1796.
[66] G. Renner, P. Kircher, G. Huttner, P. Rutsch, K. Heinze, Eur. J. Inorg. Chem. (2000) 879–887.
[67] J.D. Farwell, M.A. Fernandes, P.B. Hitchcock, M.F. Lappert, M. Layh, B. Omondi, Dalton Trans. (2003) 1719–1729.
[68] M.C.C. Ng, D.J. Craig, J.B. Harper, L. van-Eijck, J.A. Stride, Chem. Eur. J. 15 (2009) 6569–6572.
[69] M. Dräger, D. Simon, J. Organomet. Chem. 306 (1986) 183–192.
[70] K. Häberle, M. Dräger, J. Organomet. Chem. 312 (1986) 155–165.
[71] M. Weidenbruch, A. Hagedorn, K. Peters, H.G. von Schnering, Angew. Chem. Int. Ed. Engl. 34 (1995) 1085–1086.
[72] M. Weidenbruch, A. Hagedorn, K. Peters, H.G. von Schnering, Chem. Ber. 129 (1996) 401–404.
[73] A. Castel, P. Rivière, J. Satgé, H.Y. Ko, Organometallics 9 (1990) 205–210.
[74] C. Aitken, J.F. Harrod, A. Malek, E. Samuel, J. Organomet. Chem. 349 (1988) 285–291.
[75] A. Castel, P. Rivière, J. Satgé, H.Y. Ko, J. Organomet. Chem. 342 (1988) C1–C4.
[76] M. Dräger, D. Simon, Z. Anorg. Allg. Chem. 472 (1981) 120–128.
[77] K. Mochida, H. Shimizu, T. Kugita, M. Nanjo, J. Organomet. Chem. 673 (2003) 84–94.
[78] K. Mochida, H. Chiba, M. Okano, Chem. Lett. (1991) 109–112.
[79] K. Mochida, H. Chiba, J. Organomet. Chem. 473 (1994) 45–54.
[80] K. Mochida, H. Shimizu, M. Nanjo, Chem. Lett. (2000) 1226–1227.
[81] D.F. Shriver, M.A. Drezdzon, The Manipulation of Air Sensitive Compounds. John Wiley and Sons, New York, 1986.
[82] R. Schwarz, M. Lewinsohn, Chem. Ber. 64B (1931) 2352–2358.
[83] K. Mochida, N. Matsushige, M. Hamashima, Bull. Chem. Soc. Jpn. 58 (1985) 1443–1447.